Evolution of quadrupole collectivity in $N = 80$ isotones toward the $Z = 64$ subshell gap: The $B(E2; 2_1^+ \rightarrow 0_1^+)$ value of ^{142}Sm

R. Stegmann,[1,*] C. Bauer,[1] G. Rainovski,[2] N. Pietralla,[1] C. Stahl,[1] S. Bönig,[1] S. Ilieva,[1] A. Blazhev,[3] A. Damyanova,[2,4] M. Danchev,[2] K. Gladnishki,[2] J. Jolie,[3] R. Lutter,[5] J. Pakarinen,[6,7] D. Radeck,[3] E. Rapisarda,[6,8] P. Reiter,[3] M. Scheck,[9,10] B. Siebeck,[3] T. Stora,[6] P. Thöle,[3] T. Thomas,[3] M. Thürauf,[1] M. J. Vermeulen,[11] D. Voulot,[6] N. Warr,[3] F. Wenander,[6] V. Werner,[1,12] and H. De Witte[8]

[1]*Institut für Kernphysik, Technische Universität Darmstadt, D-Darmstadt, Germany*
[2]*University of Sofia, BG-Sofia, Bulgaria*
[3]*Institut für Kernphysik, Universität zu Köln, D-Köln, Germany*
[4]*University of Genève, CH-Genève, Switzerland*
[5]*Fakultät für Physik, Ludwig-Maximilians-Universität München, D-Garching, Germany*
[6]*CERN, CH-Genève, Switzerland*
[7]*University of Jyväskylä, FIN-Jyväskylä, Finland*
[8]*Instituut voor Kern- en Stralingsfysica, KU Leuven, B-Leuven, Belgium*
[9]*School of Engineering, University of the West of Scotland, Paisley, PA1 2BE, United Kingdom*
[10]*SUPA, Scottish University Physics Alliance, Glasgow, G12 8QQ, United Kingdom*
[11]*Nuclear Physics Group, Department of Physics, University of York, York, United Kingdom*
[12]*WNSL, Yale University, New Haven, Connecticut 06520, USA*

(Received 29 April 2014; revised manuscript received 1 April 2015; published 26 May 2015)

It was shown that the evolution of the $B(E2; 2_1^+ \rightarrow 0_1^+)$ values in $N = 80$ isotones from Te to Nd is affected by the underlying subshell structure. This manifests itself in the observation of the local suppression of the $B(E2)$ value at $Z = 58$ with respect to the neighboring nuclei ^{136}Ba and ^{140}Nd. To investigate this shell sensitivity toward the $Z = 64$ subshell gap, the $B(E2; 2_1^+ \rightarrow 0_1^+)$ value of the unstable nucleus ^{142}Sm was measured utilizing the projectile Coulomb excitation technique. The radioactive ion beam (RIB) experiment was performed at the REX-ISOLDE facility at CERN. The $B(E2)$ value of 32 (4) W.u. reflects the impact of the $\pi(1g_{7/2}\,2d_{5/2})$ subshell closure at $Z = 64$ with respect to a linear scaling of collectivity with valence proton number.

DOI: 10.1103/PhysRevC.91.054326 PACS number(s): 21.10.−k, 23.20.Js, 25.70.De, 27.60.+j

I. INTRODUCTION

How collectivity arises from the dynamics of the nuclear many-body system is a not fully solved problem in nuclear structure physics. The key approach to this problem is based on understanding the relations between the collective correlations and the specific single-particle structures. This is illustrated by the anticorrelation between the level energies of the 2_1^+ states in even-even nuclei and their $B(E2; 2_1^+ \rightarrow 0_1^+)$ value [1,2]. This behavior is generic between major shells indicating that low-energy quadrupole collectivity is a valence shell effect. It can be expected that the evolution of collective properties in between major shell closures should analogously be modulated by the underlying subshell structure. However, such modulations are usually smeared out by the pairing interaction. Therefore, cases where collective properties are affected by the subshell structure are interesting and may lead to refinements of nuclear models.

An example for collective states affected by the underlying subshell structure was identified in the isovector quadrupole-collective valence-shell excitations, so-called mixed-symmetry states [3], in the $N = 80$ isotones [4]. In contrast to the single isolated one-phonon $2_{1,\mathrm{ms}}^+$ states of ^{132}Te [5], ^{134}Xe [6], and ^{136}Ba [7], a fragmented $2_{1,\mathrm{ms}}^+$ state was observed in ^{138}Ce [4]. This fragmentation was ascribed to a lack of *shell stabilization* [4], a hypothesis that was supported in microscopic calculations [8]. It was concluded that the observed fragmentation is a shell effect caused by the specific subshell structure and pairing correlations.

Beyond $Z = 58$ the isovector one-phonon valence excitations were expected to be stabilized again. The proton-neutron symmetric 2_1^+ state of $^{140}_{60}\mathrm{Nd}_{80}$ can be expected to follow the overall trend of data on $N = 80$ isotones with $Z < 58$, leaving a singular deviation from this smooth evolution. Evidence for this mechanism was obtained from a recent experiment on ^{140}Nd [9]. Utilizing projectile Coulomb-excitation reactions the $B(E2; 2_1^+ \rightarrow 0_1^+)$ value was determined, confirming the suppression of the $E2$ strength in ^{138}Ce induced by the $\pi(g_{7/2})$ subshell closure: A rise of the $B(E2)$ value in ^{140}Nd with respect to the one in ^{138}Ce was discovered. Even though contemporary microscopic models cannot quantitatively account for the observed deviation, it points at a modulation of the overall trend in collectivity by the subshell structure. To explore the progression toward the $\pi(d_{5/2})$ subshell closure at

*rstegmann@ikp.tu-darmstadt.de

$Z = 64$ and its influence on low-energy quadrupole-collective states, comparable information is needed on $^{142}_{62}Sm_{80}$. In the present article we report on the result of a projectile Coulomb-excitation experiment determining the $B(E2; 2_1^+ \rightarrow 0_1^+)$ value of ^{142}Sm.

II. EXPERIMENTAL DETAILS

In the experiment reported here, a ^{142}Sm RIB was postaccelerated to 405 MeV energy exploiting the REX-ISOLDE facility [10]. This beam was shot on secondary Coulomb excitation targets surrounded by the Miniball array [11] consisting of high-purity Germanium detectors for yield measurements. The average beam intensity available for Coulomb excitation was about 10^5 pps. The ions of interest were produced by bombarding a primary target made of tantalum with 1.4-GeV protons from the PS booster at CERN. The selective ionization of the samarium atoms using RILIS [12] enhances the samarium content extracted from the primary target. After ionization, the singly charged ions are extracted, mass separated in the general purpose separator (GPS), charge bred by REX-EBIS, and then sent to the REX postaccelerator.

The accelerated cocktail RIB was impinging alternatively on 1.4 mg/cm^2-thick ^{48}Ti or 2.0 mg/cm^2 ^{94}Mo targets. The γ rays from the decay of Coulomb-excited states were detected by the MINIBALL HPGe-detector array covering approximately 2π of the solid angle. Scattered projectile and recoiling target nuclei were measured by a double-sided silicon strip detector (DSSD) [13] placed in a forward direction. The DSSD subtended an opening angle of $\theta_{lab} = 19.7°$–$58.4°$. In the case of the ^{48}Ti target foil mostly recoiling target nuclei were detected because the maximum scattering angle for the heavier projectile nuclei is 19.8°. In contrast, for the measurement on the ^{94}Mo target, the maximum scattering angle for projectile nuclei is 41.5° which allows both target and projectile nuclei to be detected in the innermost rings of the DSSD. Figure 1 shows summed γ-ray spectra, applying Doppler corrections with respect to projectile (red, solid lines) and target recoils (black, dashed lines), in coincidence with the particle signals from the DSSD. The only γ rays present in these spectra are from decays of the 2_1^+ states of ^{142}Sm (768 keV), ^{48}Ti (984 keV), and ^{94}Mo (871 keV) as well as the decay of the $3/2_1^+$ state of ^{95}Mo.

III. ANALYSIS AND RESULTS

A. Beam composition analysis

The Coulomb-excitation cross section for the 2_1^+ state of ^{142}Sm can be measured relative to the well-known cross sections for target excitations [9,14,15]. The main difficulty in this approach stems from the cocktail character of the RIB. Despite the absence of Coulomb-excitation peaks from contaminants in the spectra, the number of target excitations caused by them has to be corrected for. The presence and nature of the contaminants were determined before and after the Coulomb-excitation yield measurements by decay spectroscopy. A Bragg ionization chamber was also present in the experimental setup but the spectra from it are not conclusive. A more detailed decay spectroscopy at the end of the experiment had to be performed to quantatively evaluate the beam composition. A thick copper target placed at the target position inside MINIBALL was irradiated with the beam for 30 min. γ rays that were produced in the radioactive decay of the beam components during irradiation and within 1 h afterwards were collected in a single-event mode with MINIBALL. Figure 2 shows the singles spectra collected

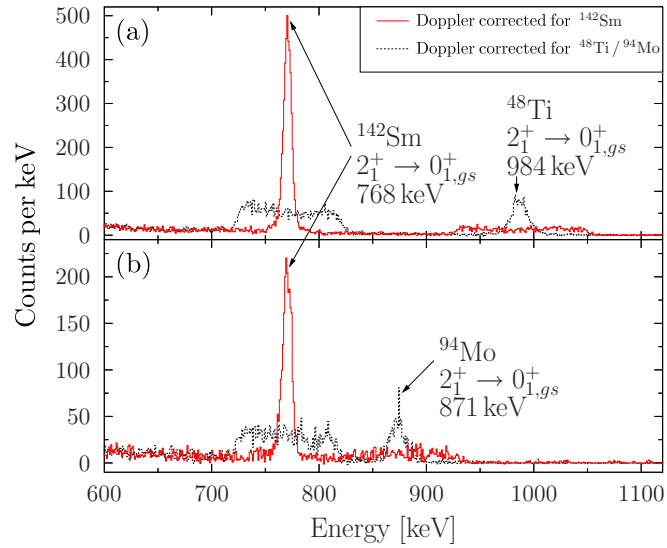

FIG. 1. (Color online) Background-subtracted particle-γ coincidence spectra Doppler corrected with respect to the projectile (red, solid line) and target (black, dashed line) recoils. (a) The spectra obtained with the ^{48}Ti target (measured for 24 h); (b) the spectra obtained with the ^{94}Mo target (measured for 8 h).

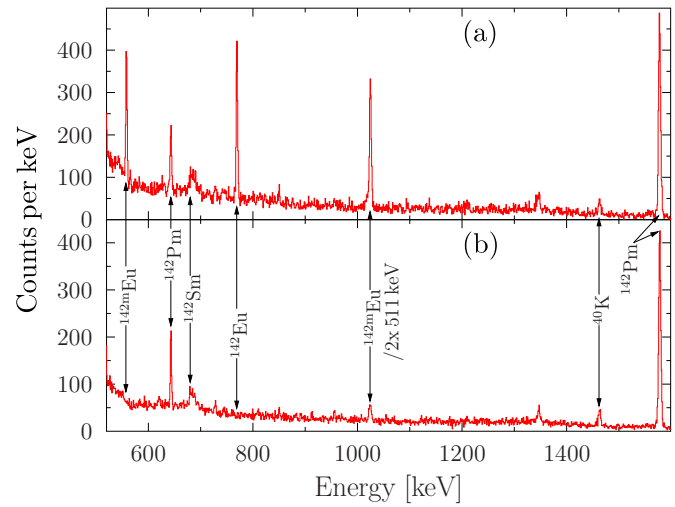

FIG. 2. (Color online) Singles spectra of the decay of projectile nuclei after the beam was collected on a thick copper target for 30 min. Several transitions belonging to the decay products of the various beam composites were observed. The spectra show the decay of the implanted ions between the first and third minutes (a) and between the 41st and 43rd minutes (b) of the decay measurement. Next to each γ-ray transition the corresponding parent nuclide is noted.

between the first and third minute [Fig. 2(a)] and between the 41st and 43rd minute [Fig. 2(b)] after the end of irradiation. Analyzing spectra recorded within these two time periods allow one to disentangle the contributions from sources with different lifetimes.

The spectra clearly show γ-ray transitions following the β^+/ EC (electron capture) decays of ^{142}Pm, ^{142g,m}Eu, and ^{142}Sm. Hence, the first two isotopes are candidates for the contaminants of the RIB used in the present experiment. The harvested activity implies that the overall fraction of isobaric contamination is about 6%–7% and cannot have a significant impact on the final result. Nevertheless, the analysis of the beam composition was performed and will be discussed in detail in the following.

The 1576-keV transition stems from ^{142}Nd, which is populated by the EC decay of ^{142}Pm. Despite the relatively short half-life of ^{142}Pm [$T_{1/2} = 40.5\,(5)$ s [16]], the relative intensity of this transition remains constant over the time period of approximately 1 h (see Fig. 2). This leads to the conclusion that all ^{142}Pm nuclei are produced in the decay of the longer-lived ^{142}Sm, i.e., the beam consists only of ^{142g,m}Eu and ^{142}Sm, which follows the β^- decay of ^{142}Eu. The presence of ^{142}Eu is indicated by the observed $2_1^+ \rightarrow 0_1^+$ transition in ^{142}Sm at 768 keV. However, the occurrence of decay lines at 556 keV as well as 1023 keV imply also the presence of ^{142m}Eu, because these transitions do not occur in the ground-state decay of ^{142g}Eu.

Because ^{142}Eu is present in the nuclear ground state [1^+, $T_{1/2} = 2.34\,(12)$ s [16]] as well as in the excited isomeric state [8^- at 460 keV, $T_{1/2} = 1.223\,(8)$ min [16]] it is necessary to estimate the isomeric ratio. The 768-keV transition ($2_1^+ \rightarrow 0_1^+$ in ^{142}Sm) is produced in either of these two decays. As far as the lifetimes of the isomeric and ground-state decay of ^{142}Eu differ by two orders of magnitude, the isomeric ratio can be estimated by fitting the decay curve of the 768-keV transition with two components corresponding to the respective lifetimes. This analysis leads to an isomeric ratio of $N(^{142m}\mathrm{Eu})/N(^{142g}\mathrm{Eu}) = 23.5\,(94)\,\%$.

The two orders of magnitude difference between the half-life of $T_{1/2} = 1.223\,(8)$ min in ^{142m}Eu compared to $T_{1/2} = 72.49\,(5)$ min of ^{142}Sm [16] render decay spectroscopy after ending irradiation as unsuitable for the contamination analysis because the decay process for most of ^{142m}Eu already took place during the 30-min irradiation. To resolve this challenge we had to examine the spectra collected in the process of irradiation of the thick copper target.

REX delivered a pulsed beam with a pulse length of $\xi_a \approx 200\,\mu$s and a repetition rate of $6\frac{2}{3}$ Hz resulting in a period of $\xi = 150$ ms and a span of $\xi_b = 149.8$ ms in between two pulses. During the latter only the radioactive decay of ions implanted beforehand takes place at rate,

$$\frac{dN(t)}{dt} = -\lambda N(t), \tag{1}$$

where $N(t)$ is the absolute number of nuclides of one species (either ^{142}Eu or ^{142}Sm in this case) present in the implantation foil while λ denotes the respective decay constant. During a pulse of length τ_a the decay rate amounts to

$$\frac{dN(t)}{dt} = \dot{M} - \lambda N(t), \tag{2}$$

where $\dot{M}$ denotes the beam intensity averaged over a single beam pulse. A full period of $\xi = 150$ ms starts with a pulse [see Eq. (2)] which is successively followed by a time without beam [see Eq. (1)]. Solving this set of coupled differential equations yields recursive expressions for both cases that can be expressed as geometric series. Using the known convergence into saturation the solution after k fully elapsed periods ξ of irradiating the target can be written as

$$N(k\xi) = \frac{\dot{M}}{\lambda}\,(1 - e^{-\lambda\xi_a})\,e^{-\lambda\xi_b}\,\frac{1 - e^{-\lambda k\xi}}{1 - e^{-\lambda\xi}}. \tag{3}$$

For the case of large irradiation times $t \gg \xi$ (here, minutes vs milliseconds) it holds that $k \gg 1$ leading to the conclusion that the difference of intervals with and without beam are negligible in matters of count rate permitting one to assume $k\xi \approx t$. The decay activity is then written as $A(t) = \lambda N(t) \approx \dot{M}(1 - e^{-\lambda\xi_a})e^{-\lambda\xi_b}(1 - e^{-\lambda t})/(1 - e^{-\lambda\xi})$. Because this is only valid for large irradiation times it must be integrated over the entire time of irradiation T, resulting in $N_\gamma(T) = \int_0^T A(t)dt$. This equation then allows one to calculate the amount of one ion species inside one beam pulse averaged over the time T from the full spectrum, summed over the time of irradiation:

$$\dot{M} = \frac{N_\gamma(T)(e^{-\lambda\xi} - 1)}{(1 - e^{-\lambda\xi_a})\,e^{-\lambda\xi_b}\left[T + \frac{1}{\lambda}\,(e^{-\lambda T} - 1)\right]}. \tag{4}$$

Inserting the transition intensities following the decay from Table I into Eq. (4) for ^{142m}Eu as well as for ^{142}Sm enables us to express the ratio of both isobaric components of the beam by

$$\frac{\dot{M}_{^{m}\mathrm{Eu}}}{\dot{M}_{\mathrm{Sm}}} = \frac{N_{\gamma,^{m}\mathrm{Eu}}}{N_{\gamma,\mathrm{Sm}}} \times \frac{T + \frac{1}{\lambda_{\mathrm{Sm}}}(e^{-\lambda_{\mathrm{Sm}}T} - 1)}{T + \frac{1}{\lambda_{^{m}\mathrm{Eu}}}(e^{-\lambda_{^{m}\mathrm{Eu}}T} - 1)} = 2.0\,(16)\,\%. \tag{5}$$

Repeating this procedure for the ratio of ^{142}Eu to ^{142}Sm yields $\dot{M}_{\mathrm{Eu}}/\dot{M}_{\mathrm{Sm}} = 6.7\,(60)\,\%$. While the uncertainty of this ratio is large it is obvious that the absolute contamination of the ^{142}Sm beam by ^{142}Eu ions is smaller than 15%.

The decay spectroscopy is not sensitive to the presence of stable isotopes in the beam. Therefore to estimate the possible contributions of the stable isobars ^{142}Ce and ^{142}Nd we used

TABLE I. Intensities of transitions following radioactive decay of ^{142g}Eu, ^{142m}Eu, and ^{142}Sm for determination of their respective beam fraction. The intensities have been determined from γ-ray spectra collected during the irradiation time of 30 min. The intensities for ^{142g}Eu and ^{142m}Eu were estimated using the isomeric ratio.

Nuclide	Half-life $T_{1/2}$	Energy / keV	N_γ (Counts for 30 min)
^{142g}Eu	2.34 (12) s	768.0 (2)	$2.5\,(10) \times 10^4$
^{142m}Eu	1.223 (8) min	768.0 (2)	$7.2\,(10) \times 10^3$
^{142}Sm	72.49 (5) min	679 (1)	$5.5\,(44) \times 10^4$

TABLE II. Summary of the detected γ-ray yields with particle coincidence for the ^{48}Ti target, corrected for γ-ray efficiency and beam impurities.

θ_{lab} range	Ring (DSSD)	Detected	^{142}Sm	^{48}Ti
30.8°–39.7°	4–6	Target	777 (24)	243 (21)
39.8°–46.9°	7–9	Target	814 (25)	292 (24)
47.0°–52.6°	10–12	Target	762 (24)	309 (25)
52.6°–57.1°	13–15	Target	644 (22)	249 (21)

the data from Coulomb excitation runs on the ^{48}Ti target. The expected number of counts per incident ion in the $2_1^+ \rightarrow 0_1^+$ transitions of ^{142}Ce and ^{142}Nd were estimated using CLX and DCY codes [17] and fitted to experimental spectra using a G-test approximation [18]. The procedure yields an upper limit for the beam contamination of 1% in the case of ^{142}Nd and 0.6% in the case of ^{142}Ce, respectively. The total beam contamination of all four isobaric contaminants (^{142}Eu, ^{142m}Eu, ^{142}Nd, and ^{142}Ce) adds up to 8.8 (62)%. The main impact of the contaminants is an increase in statistical uncertainty of the measured intensities from target excitation.

Another issue related to the determination of the Coulomb excitation yields arises for the measurement with the ^{94}Mo target. This target was enriched to 94.2 (30) %. In the excitation spectra obtained with this target γ rays from ^{95}Mo were observed. The Coulomb-excitation yields of the projectiles were corrected by a factor of 5.8 (30)% according to the excitation yields for ^{95}Mo. The final Coulomb-excitation yields that are only from Coulomb interaction between the ^{142}Sm beam and the ^{48}Ti and the ^{94}Mo targets are presented in Tables II and III, respectively.

B. Extraction of the matrix elements

Those events have been selected for further analysis where target nuclei have been detected to recoil into the polar angle ranges θ_{lab} = 30.8°–39.7°, 39.8°–46.9°, 47.0°–52.6°, and 52.6°–57.1°. Various angular ranges were defined to maximize sensitivity for both relevant matrix elements, M_{20} and M_{22}. The angular ranges for the particle gates had to be reassigned in the case of the ^{94}Mo target because of significant difference in kinematics. The Coulomb-excitation cross section $\sigma(2_1^+)$ depends on the $2_1^+ \rightarrow 0_1^+$ transitional matrix element M_{20} and on the quadrupole moment of the 2_1^+ state via the diagonal matrix element M_{22}. Both quantities are well known for the ^{94}Mo and ^{48}Ti target nuclei. The projectile-excitation cross section can be retrieved from the target-excitation cross section

TABLE III. Summary of the detected γ-ray yields with particle coincidence for the ^{94}Mo target, corrected for γ-ray efficiency, beam, and target impurities.

θ_{lab} range	Ring (DSSD)	Detected	^{142}Sm	^{94}Mo
30.8°–39.7°	4–6	Projectile	640 (29)	233 (20)
30.8°–42.3°	4–7	Target	387 (21)	139 (14)
44.8°–57.1°	9–15	Target	386 (21)	138 (14)

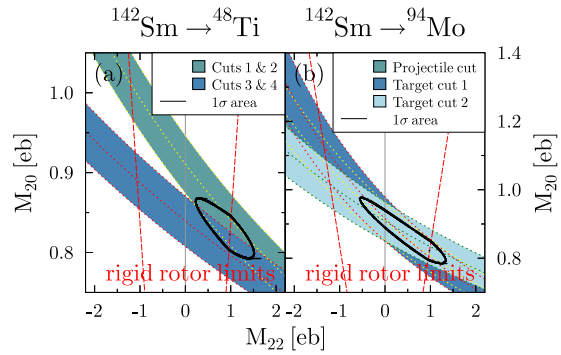

FIG. 3. (Color online) Results of the "maximum likelihood" analysis for ^{142}Sm. (a) Result of the measurement on ^{48}Ti. The bands from cuts 1 and 2 as well as 3 and 4 on the detected recoiling target nuclei are pairwise combined to restrain statistical errors resulting in a reduced one sigma area. (b) The same situation but with ^{94}Mo as the target material. In this case it was possible to gate on recoiling target as well as projectile nuclei so that three gates could be set.

and the ratio of the respective experimental yields for each gate on the detected particles separately.

By varying both matrix elements a map of projectile cross sections is computed using the computer codes CLX and DCY [17]. Comparison to the aforementioned projectile-excitation cross section allows one to retrieve sets of consistent matrix elements. Taking also the uncertainties into account and performing the analysis for each particle gate separately yields the bands shown in Fig. 3. Superposition of the bands retrieved in combination with a maximum-likelihood analysis results in a 1σ area highlighting the most probable set of matrix elements. The procedure for this maximum-likelihood analysis is explained in detail in Refs. [9,14,19].

For this particular data set very large quadrupole matrix elements, larger than 3 eb, would not be excluded at this level of statistical significance without further constraints for a relation between the $B(E2)$ value and the quadrupole moment. To slightly constrain the data by physical insight we require the quadrupole moment to be at least not much larger than the rigid rotor limit. This is achieved by exponentially reducing the likelihood of a set of matrix elements with a quadrupole moment outside of the rigid rotor limit. The analysis yields M_{20} = 0.83 (4) eb in the case of the ^{48}Ti target and M_{20} = 0.88 (10) eb for the ^{94}Mo target, respectively. It is evident that the measurements with the two different targets are in very good agreement. The error-weighted average of both measurements then gives $B(E2; 0_1^+ \rightarrow 2_1^+)$ = 0.70 (9) e^{2}b^2 corresponding to $B(E2; 2_1^+ \rightarrow 0_1^+)$ = 32 (4) W.u.

IV. DISCUSSION

The evolution of the $B(E2; 2_1^+ \rightarrow 0_1^+)$ strengths in the $N = 80$ isotones as a function of the proton number is shown in Fig. 4. This figure is an extension of Fig. 6 from Ref. [9], including the present result for ^{142}Sm. The newly measured $B(E2)$ value of ^{142}Sm is comparable to that of ^{140}Nd and deviates significantly from the $N_\pi N_\nu$ behavior (shown as dotted line in Fig. 4; for details see [9]). It exhibits

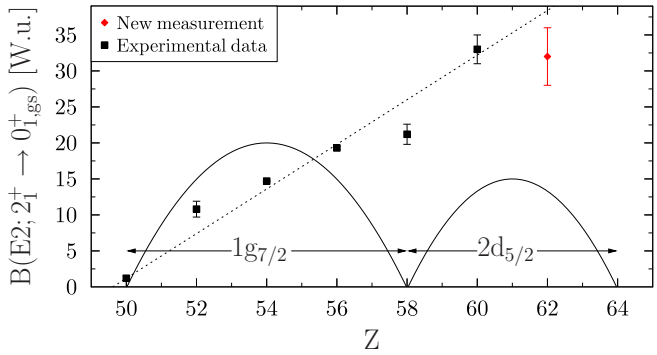

FIG. 4. (Color online) Evolution of the $B(E2;2_1^+ \rightarrow 0_1^+)$ values in the $N = 80$ isotonic chain. Between $Z = 50$ and $Z = 62$ the proton $1g_{7/2}$ and $2d_{5/2}$ orbitals are consecutively filled. The experimental data are taken from [4,5,9,20–22]. The value for ^{140}Nd [9] was determined in another experiment in the same experimental campaign.

the expected decrease toward the $Z = 64$ subshell closure. This is in qualitative agreement with the hypotheses that the general trend of quadrupole collective properties ($N_\pi N_\nu$ behavior) are modulated by the underlying subshell structure as suggested in Ref. [9]. Again, like in the case of ^{140}Nd [9], the contemporary microscopic nuclear models can reproduce only the general increasing trend but are not able to account for the observed modulations. The quasiparticle-phonon model predicts for the $B(E2;2_1^+ \rightarrow 0_1^+)$ strengths in ^{142}Sm a value of 22 W.u. [8]. Like in the case of ^{140}Nd, it underestimates the experimental value in ^{142}Sm. The large-scale shell model gives a value of 27.4 W.u. [23] in agreement with the data on ^{142}Sm within uncertainties. At the same time the large-scale shell model underestimates the value for ^{140}Nd. Further efforts, experimental and theoretical, are needed toward an understanding of this phenomenon.

ACKNOWLEDGMENTS

We gratefully acknowledge the support of the staff members at CERN during the experimental runs, in particular Emiliano Piselli and Miguel Benito. G. Rainovski acknowledges support from the Alexander von Humboldt foundation. This experiment was supported by the BMBF under Grants No. 05P09RDCI6, No. 05P12RDCIB, No. 05P12RDFN8, No. 06DA9036I, No. 05P12RDCIA, No. 05P09PKCI5, No. 05P12PKFNE, and No. 06KY9136I; HIC for FAIR funded by the State of Hesse in the framework of the LOEWE program; the DAAD German-Bulgarian exchange program; U.S. Department of Energy Grant No. DE-FG02-91ER-40609, and ENSAR.

[1] S. Raman, C. Nestor Jr., and P. Tikkanen, At. Data Nucl. Data Tables **78**, 1 (2001).
[2] L. Grodzins, Physics Letters **2**, 88 (1962).
[3] F. Iachello, Phys. Rev. Lett. **53**, 1427 (1984).
[4] G. Rainovski *et al.*, Phys. Rev. Lett. **96**, 122501 (2006).
[5] M. Danchev *et al.*, Phys. Rev. C **84**, 061306 (2011).
[6] T. Ahn *et al.*, Phys. Lett. B **679**, 19 (2009).
[7] N. Pietralla *et al.*, Phys. Rev. C **58**, 796 (1998).
[8] N. Lo Iudice, C. Stoyanov, and D. Tarpanov, Phys. Rev. C **77**, 044310 (2008).
[9] C. Bauer *et al.*, Phys. Rev. C **88**, 021302 (2013).
[10] O. Kester *et al.*, Nucl. Instrum. Methods Phys. Res. B **204**, 20 (2003).
[11] N. Warr *et al.*, Eur. Phys. J. A **49**, 40 (2013).
[12] V. Fedosseev *et al.*, Nucl. Instrum. Methods Phys. Res. B **266**, 4378 (2008).
[13] A. Ostrowski *et al.*, Nucl. Instrum. Methods Phys. Res. A **480**, 448 (2002).
[14] A. Ekström *et al.*, Phys. Rev. C **80**, 054302 (2009).
[15] C. Bauer *et al.*, Phys. Rev. C **86**, 034310 (2012).
[16] T. Johnson *et al.*, Nuclear Data Sheets **112**, 1949 (2011).
[17] H. Ower, Ph.D thesis, Goethe University Frankfurt, 1980.
[18] R. R. Sokal and F. J. Rohlf, *Biometry: The Principles and Practice of Statistics in Biological Research*, 2nd ed. (Freeman, New York, 1981).
[19] J. Beringer *et al.* (Particle Data Group), Phys. Rev. D **86**, 010001 (2012).
[20] D. Radford *et al.*, Nucl. Phys. A **746**, 83 (2004).
[21] G. Jakob *et al.*, Phys. Rev. C **65**, 024316 (2002).
[22] M. J. Bechara, O. Dietzsch, and J. H. Hirata, Phys. Rev. C **29**, 1672 (1984).
[23] D. Bianco, F. Andreozzi, N. Lo Iudice, A. Porrino, and F. Knapp, Phys. Rev. C **85**, 034332 (2012).